A numerical tool to calculate ion mobility at arbitrary fields from all-atom models.

Viraj D. Gandhi[1,2], Kyle Short[1], Leyan Hua[1], Iván Rodríguez [1], Carlos Larriba-Andaluz[1,*]

[1]Department of Mechanical Engineering, Indiana University-Purdue University, SL 260, 723 W. Michigan Street, Indianapolis, Indiana, USA

[2]Department of Mechanical Engineering, Purdue University, 585 Purdue Mall, West Lafayette, Indiana, USA

A technical note to be submitted to the Journal of Aerosol Science

*corresponding author. Email: clarriba@iupui.edu

Postal address: SL 260, 723 W. Michigan Street, Indianapolis, IN 46202

Abstract

In an effort to calculate electrical mobilities in the free molecular regime using electrical fields that are non-negligible, an algorithm based on the calculation of collision integrals and the two-temperature theory has been created and tested. The algorithm calculates the mobility based on the effective temperature of the ion using a 4-6-12 potential interaction with or without an ion-quadrupole potential (for the case of nitrogen gas). The ion's energy is also approximated so that a relation between the effective temperature of the ion and the field over concentration may be given. The algorithm is parallelized and tested against experimental results for small ions in light gases successfully. The algorithm has also been tested in nitrogen for mid-sized analytes at room temperature and at 100K despite the fact that the inelasticity of collisions has not yet been considered. At 100K, the reduction of the capture radius with the increase of the electric field is apparent for many of the analytes producing "humps" in the reduced mobility vs. the field over concentration curve. For the smallest ions, two humps are observed. One pertaining to the dispersion forces and a second one due to the ion-induced dipole interaction.

Keywords: ion mobility; IMoS; high field; Collision Cross Section; two-temperature theory.

1. Introduction

Ions in the gas phase can be separated by means of their electrical mobility. The main empirical method of separation uses a well-known electric field that accelerates the ions through a buffer gas. Eventually, the ions reach a drift velocity v_d that can be related to the electrical mobility K and electrical field E as(McDaniel & Mason, 1973; Viehland & Viehland, 2018):

$$v_d = KE \tag{1}$$

Experimentally, it is reasonably simple to obtain the value of mobility for an ion of any shape making the technique very useful to separate ions. Obtaining the mobility theoretically or numerically is quite a difficult task as the mobility depends on a large number of parameters, including shape, gas density, gas temperature, ion-neutral potential interaction, field employed as well as the mass of both the ion and the gas or even the center of mass and moment of inertia of the ion gas pair.

In an effort to improve the theory and numerical calculations of electrical mobility, the authors created a suite of algorithms named Ion Mobility Spectrometry Suite (IMoS) that uses all-atom models and a multitude of potential interactions to calculate mobility(Coots, Gandhi, Onakoya, Chen, & Andaluz, 2020). The calculations were all based on the assumption that the drift velocity was much smaller than the thermal velocity of the gas, or seemingly that interaction happened for vanishing fields ($E \to 0$). However, there are many recent and old instruments where this condition is stretched or is not at all valid. For example, technologies like Differential Mobility Spectrometry (DMS), Field Asymmetric Waveform Ion Mobility Spectrometry (FAIMS) or T-wave make use of fields over concentrations than can exceed hundreds of Td(Dodds & Baker, 2019; Gabelica & Marklund, 2018). Even under some circumstances, the Differential Mobility Analyzer (DMA) can reach tens of Td(Rus et al., 2010). The effect of high fields on mobility is complicated and many times it cannot be neglected.

In this technical note, the authors make use of the two-temperature theory to create an additional algorithm to IMoS that provides calculations at high fields(V. Gandhi, 2022; Viehland & Mason, 1975, 1978). The two-temperature theory, as its name suggests, assumes that, due to the ion's heating, its effective temperature increases over that of the gas in a fashion directly related to the field over concentration. The calculation is based on approximations to the moments of the Boltzmann equation, which have been implemented in the code up to the fourth approximation(V. Gandhi, 2022).

The algorithm comes with a modified manual that explains how to perform these calculations followed by typical examples which have been added to the supplementary information. The method has been tested

previously for all-atom models in light gases successfully providing very good agreement with experimental results(V. D. Gandhi & Larriba-Andaluz, 2021). While the method can also be applied to heavier gases like nitrogen or air, any possible inelasticity that will arise from the collision is not accounted for at this time. This inelasticity is expected to be important only at high fields, and as such, an approximation can still be made without incurring in excessive error, in particular when a correction is made to account for it. A brief explanation of the two-temperature theory is provided below with a comparison of the results for different ions in helium and nitrogen.

2. Theory

If the ion's velocity distribution was known for a particular applied electric field in a gas of density n and temperature T, it would be straightforward to calculate the drift velocity and hence the mobility by just taking the appropriate average. In momentum transfer theory, the ion's velocity distribution F is many times assumed, as in the work of Epstein, Mackowski, or Rosner(Epstein, 1924; Garcia- Ybarra & Rosner, 1989; Mackowski, 2006). The distribution is then linearized (Chapman-Enskog's approximation(Chapman & Cowling, 1970)) and the drag force/mobility is calculated. However, one of the assumptions is that the ion's velocity is very small, and that the ion's temperature is the same as that of the gas. The approximation is therefore only valid at low to vanishing fields and for masses of the ion that are large compared to the mass of the gas. In the case of ions at high velocity or under the effects of strong fields, the momentum transfer theory assumption of the distribution breaks. In order to calculate the ion's distribution, or a moment of it, the Boltzmann equation must be solved by assuming a different (and higher) temperature for the ion(Kruger & Vincenti, 1965):

$$\frac{qeE}{Mn}\frac{\partial F}{\partial z_1} = \int\int\int (f'F' - fF) g\, b db d\epsilon d\vec{c} \tag{2}$$

Here, M and qe are the mass and the charge of the ion, respectively, f is the gas velocity distribution (assumed Maxwellian), $\vec{g} = \vec{z} - \vec{c}$ is the relative velocity vector with $\vec{z} = (z_1, z_2, z_3)$ and $\vec{c}$ being the velocity of the ion and gas respectively and where $d\vec{c}$ stands for $dc_1 dc_2 dc_3$. b is the impact parameter and ϵ is the intrinsic rotation angle. The collision term on the right-hand side describes the typical replenishment and extinguishment of velocities of ions of class z_i through collisions with the gas summed over all possible gas velocities and orientations. Several assumptions have been made to arrive at eq. (2), being the most significant that the ion does not perturb the gas Maxwellian distribution, that the collisions are assumed translationally elastic, and that the ion density N is much smaller than that of the gas n. In the case of the two-temperature theory, the condition imposed on the solution is that the temperature of the ion might be different from that of the gas due to heating. The distribution can be approximated by:

$$F = F^{(0)} \sum_p a_p \phi_p = \left(\frac{M}{2\pi k T_b}\right)^{\frac{3}{2}} e^{-\frac{M(z)^2}{2kT_b}} \sum_p a_p \phi_p \tag{3}$$

Here $F^{(0)}$ is the zero-basis distribution and the sum represents an infinite sum of orthogonal functions ϕ_p and coefficients a_p. Note that the basis function depends on a base temperature $T_b \neq T$. This temperature normally is assumed to be the ion's temperature in the lab frame of reference. While the distribution itself is difficult to calculate, approximations to moments of the distribution can be obtained through recursiveness relations of the orthogonal functions - Burnett functions in the case of the two-temperature theory- whose averages are related to the moments of the distribution. The mobility can therefore be calculated through the velocity moment of the distribution at different levels of approximation. For the first approximation, the calculation yields the Mason – Schamp equation (Viehland & Mason, 1975):

$$\langle K \rangle_I = \frac{3}{16}\frac{qe}{n}\left(\frac{2\pi}{\mu k T_{eff}}\right)^{\frac{1}{2}} \frac{1}{\bar{\Omega}_{T_{eff}}(1,1)} \tag{4}$$

Where μ is the reduced mass, k is the Boltzmann constant, T_{eff} is the effective temperature and $\bar{\Omega}_{T_{eff}}(1,1)$ is the averaged momentum collision integral calculated at the effective temperature and normally referred to as the Collision Cross Section (CCS). The effective temperature is related to T_b through the relation:

$$T_{eff} = \frac{MT+mT_b}{M+m} \tag{5}$$

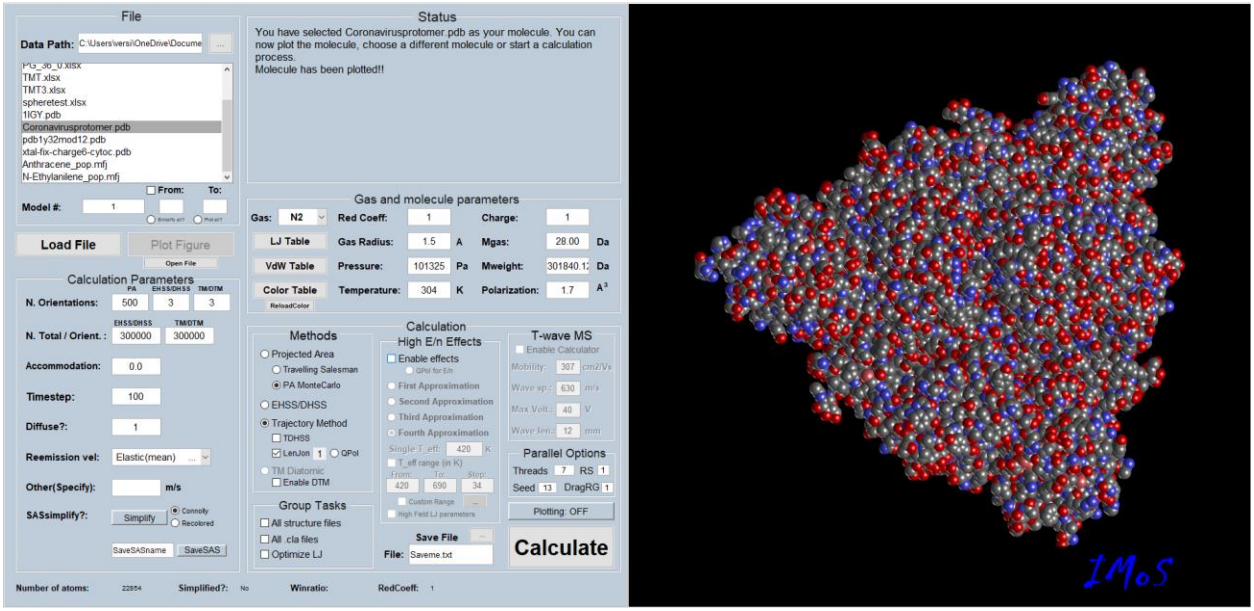

Figure 1. IMoS v1.12 interface with the Coronavirus Protomer plotted.

Higher order approximations may also be obtained by adding a series of corrections that depend on even powers of the field over the concentration (E/n), so that the mobility is a symmetric function of the field. For example, for the 4th approximation:

$$\langle K\rangle_{IV} = \langle K\rangle_I \left(1 + \alpha_0 + \alpha_1 \left(\frac{E}{n}\right)^2 + \alpha_2 \left(\frac{E}{n}\right)^4 + \alpha_3 \left(\frac{E}{n}\right)^6\right) \tag{6}$$

Here the $\langle K\rangle_I$ represents the first approximation (eq. 4) and the α_i coefficients are convoluted functions of collision integrals $\bar{\Omega}_{T_{eff}}(l,s)$. The collision integrals in general are given by(Mason & Schamp Jr, 1958):

$$\Omega(l,s)(T_{eff}) = \frac{2}{(s+1)!}\left(\frac{\mu}{2k_bT_{eff}}\right)^{s+2} \int_0^\infty e^{-\left(\frac{\mu}{2k_bT_{eff}}\right)g^2} g^{2s+3} Q^{(l)}(g)dg \tag{7}$$

$$Q^{(l)} = 2\pi\left(\frac{2(l+1)}{2l+1-(-1)^l}\right)\int_0^\infty (1-\cos^l\chi(b))bdb \tag{8}$$

Where χ is the deflection angle of the gas molecule as it interacts with the ion. This deflection angle depends on the potential interactions between ion and gas which must be calculated numerically(Mesleh, Hunter, Shvartsburg, Schatz, & Jarrold, 1996). However, once the deflection angle is obtained for a sufficient number of trajectories, any collision integral, in particular the momentum transfer CCS pertaining to the first approximation, may be calculated. To obtain the α_i coefficients and higher order approximations, an ancillary relation between the base temperature T_b (or T_{eff}) and E/n is needed. This relation can be obtained by solving the ion's energy moment, which can also be solved at different degrees of approximation. Assuming that the base temperature is related directly to the ion's energy, a general expression can be written as(V. Gandhi, 2022; Viehland & Mason, 1975, 1978):

$$\frac{1}{2}M\langle z^2\rangle = \frac{3}{2}kT_b = \frac{3}{2}kT + \frac{1}{2}M\langle z\rangle^2 + \frac{1}{2}m\langle z\rangle^2(1+\beta) \tag{9}$$

and where $\langle z \rangle = v_d = KE$ is the drift velocity and β includes corrections from higher approximations. Eq. (9) is sometimes referred to as the Wannier equation when $\beta = 0$(Wannier, 1953). The Wannier expression provides a clear account of what the ion's energy entails. $\frac{3}{2}kT_b$ refers to the ion's total translational energy and includes the macroscopic kinetic energy from the field $\frac{1}{2}M\langle z \rangle^2 = \frac{1}{2}Mv_d^2$. On the other hand, $\frac{3}{2}kT_{eff} = \frac{3}{2}kT + \frac{1}{2}m\langle z \rangle^2$ corresponds to the translational molecular energy which includes the equilibrium energy of the gas bath plus a collisional term that causes the ion to heat up, $\frac{1}{2}m\langle z \rangle^2$. Hence the effective temperature is the expected thermodynamic temperature of the ion. Finally, the effective energy can be related to the relative kinetic energy of the ion and the gas, providing a second perspective to its meaning. Overall, eq. (6) can be calculated together with eq. (9) to provide the desired level of approximation for the calculation of mobility. An important characteristic of the two-temperature theory is all approximation terms are bounded, meaning that any degree of approximation converges for the full range of the field-over-concentration E/n, including the first approximation, and where the merit of higher approximations is to obtain greater accuracy(McDaniel & Mason, 1973).

A particular issue of concern with the two-temperature theory is the assumption of elastic collisions between gas and ion in the translational sense (relative kinetic energy is kept constant). While the theory is expected to work well for monoatomic gases, the expectancy is that collisions with polyatomic gases will be somewhat inelastic as some of the extra energy of the ion (which is heated up) can go into the internal and rotational degrees of the gas molecule and thus, the relative kinetic energy is not kept constant. In such occurrences, a correction must be made to the equations. These corrections have not been yet implemented as they can only be obtained experimentally at this time and an error is expected for polyatomic gases and high fields of a few percent.

3. Methods

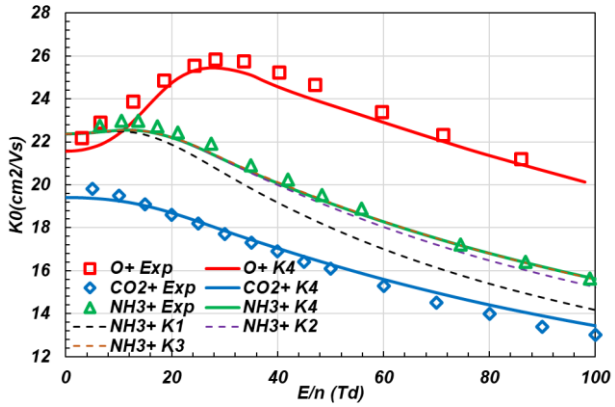

Figure 2. Reduced Mobility as a function of the field-over-concentration (E/n) for three small ions in He. The markers correspond to experimental data while the solid lines correspond to the fourth approximation of the two-temperature theory. For CH_5^+, dashed lines show the first through third approximations.

IMoS v1.12 interface is shown in Figure 1(Larriba-Andaluz, Fernandez-Garcia, Ewing, Hogan, & Clemmer, 2015; Larriba & Hogan Jr, 2013a, 2013b; Shrivastav, Nahin, Hogan, & Larriba-Andaluz, 2017). In it, various calculations pertaining to the prediction of mobility can be performed(Donald & Prell, 2019). Most of such calculations are parallelized and can be run on a supercomputer with ease, greatly increasing performance. The new additional calculations can be found at the center of the Calculation pane pertaining to high-field effects. The program loads an all-atom structure like the one depicted in Figure 1. It then calculates the deflection angle of a selected number of gas trajectories (default is 900000 trajectories) at a fixed gas temperature and at an effective temperature of the ion. To calculate the angle, a 4-6-12 potential interaction is assumed which includes the ion-induced dipole potential for the gas of choice and the

pertaining Lennard-Jones interactions that are typical of the Trajectory Method(Mesleh et al., 1996). If nitrogen is chosen, there is also the possibility of adding the ion-quadrupole potential interaction(Kim et al., 2008). Once the deflection angle is calculated, the program then obtains the necessary α_i coefficients up to the fourth approximation. It also calculates the relation between T_{eff} and E/n by determining the ion's energy moment, which is obtained at the same accuracy as the mobility. The calculation is normally carried out for a range of effective temperatures to provide a relation between the ion's mobility and the field-over-concentration (E/n). The results are then provided in an output file, including the CCS. The algorithm comes with a manual that describes the calculations in detail, including how to create the initial files and provides several examples of how to do the high-field calculations through the interface or via a submission to a supercomputer through a non-interface version.

It is important to mention that the calculation does not include any possible inelasticity effects at this time(V. Gandhi, 2022; Larriba-Andaluz, 2021), which are expected to be included at a later stage. In principle, as the relative energy of ion and gas increases, the expectancy is that the collisions become inelastic in the translational energy sense, providing energy to internal degrees of freedom. For monoatomic gases and light ions, this is not particularly important as the ion will rapidly arrive at an equilibrium temperature and no modes of escape (the gas does not have internal degrees of freedom) are available except for perhaps radiation. For polyatomic gases, on the other hand, translational energy can be lost into the degrees of freedom of the gas molecule (which is at the gas temperature), providing inelastic mechanisms that will affect the momentum transfer.

4. Results and Discussion

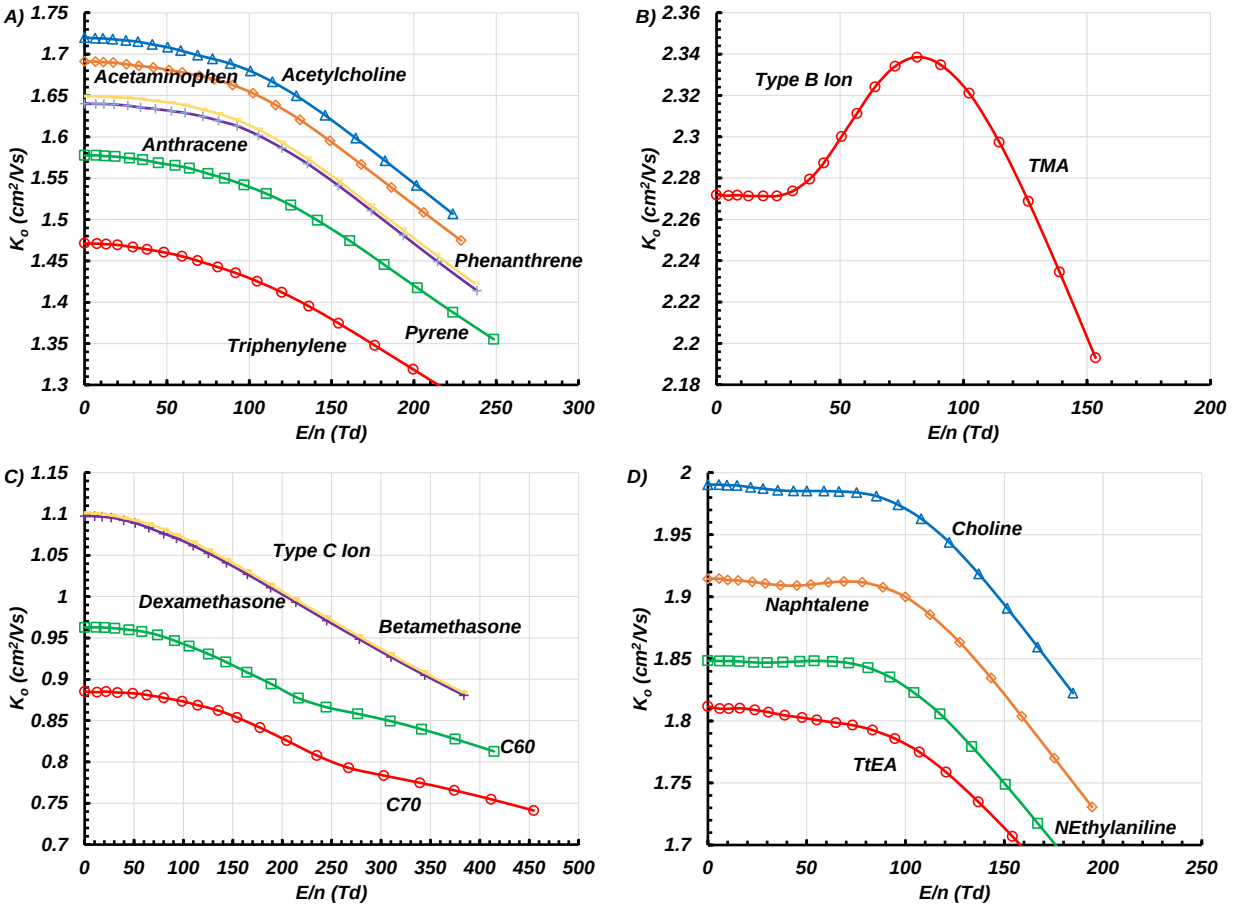

Figure 3. Reduced Mobility as a function of field over concentration of several different ions in nitrogen at gas temperature of 300K. The values correspond to the numerical calculations of the fourth approximation to the two-temperature theory.

The two-temperature theory for all-atom models and light gases has been tested previously for small ions in light gases. The theory is able to reproduce the results quite well even for the first approximation without any type of optimization of the Lennard-Jones potentials. Figure 2 reproduces some of the results for small ions in He where the reduced mobility is plotted as a function of the field over concentration for three ions. The markers represent experimental results while the solid lines represent the fourth approximation to the two-temperature theory. For the NH_3^+ ion, approximations one through four are shown, and where the best agreement between experiments and theory occurs for the fourth approximation. However, for the range of field over concentration shown, there is little difference between the third and fourth approximation, hinting at only small gains for even higher approximations.

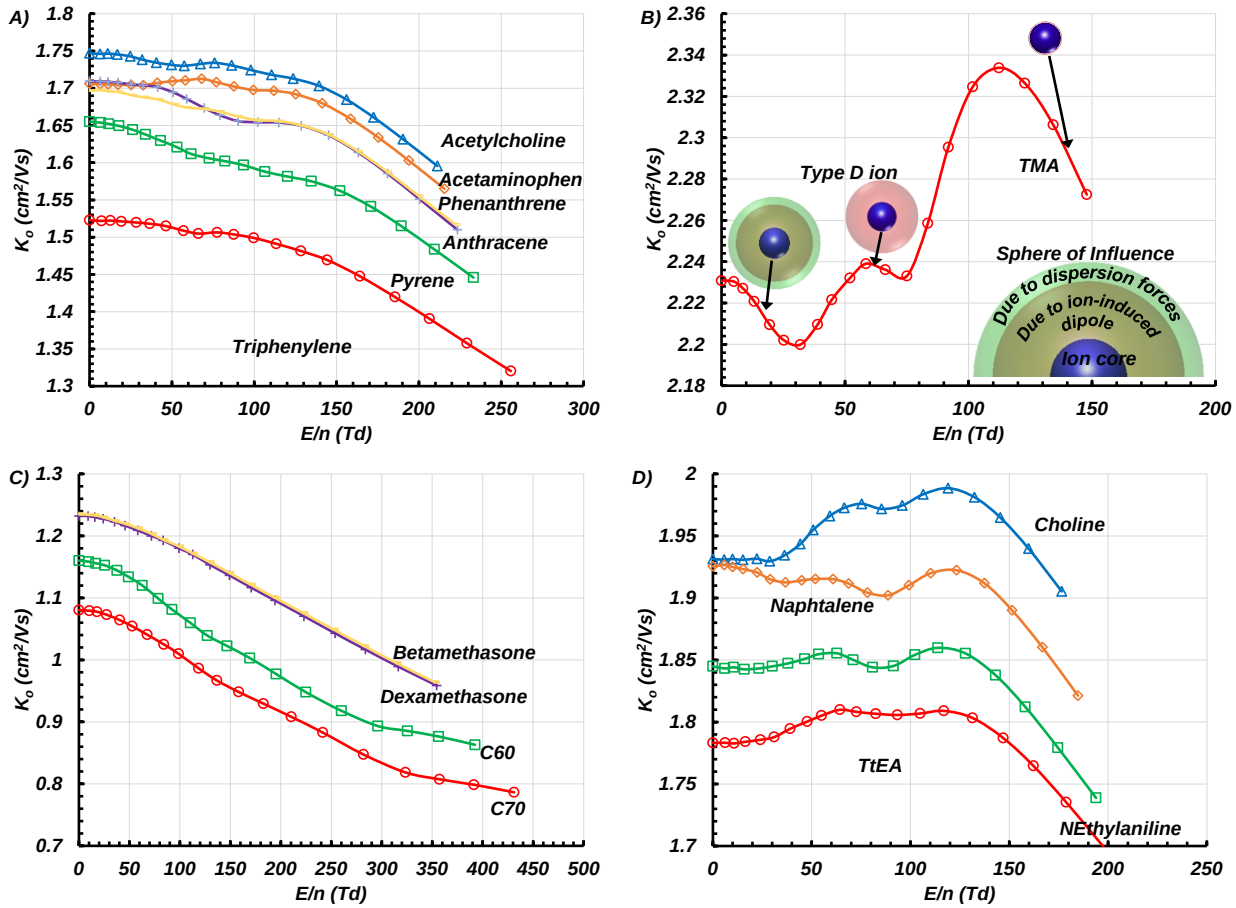

Figure 4. Reduced Mobility as a function of field over concentration of several different ions in nitrogen at gas temperature of 100K. The values correspond to the numerical calculations of the fourth approximation to the two-temperature theory. Noteworthy is the double hump that can be observed in some of the ions.

While successful for small ions in light gases, the algorithm can run at different fields for different gas temperatures for heavier gases very efficiently and for which very few experimental results exist. To showcase the results, a series of tests on typical analytes in nitrogen have been performed. The results from the 4th approximation are shown in Figure 3 for a gas temperature of 300K. Reduced mobility is used on the ordinate axis which is generally given by:

$$K_0 = K\left(\frac{P}{101325}\right)\left(\frac{273.15}{T}\right) \tag{10}$$

Where P and T are the pressure and temperature of the gas. How the mobility of ions behave at high fields has been studied extensively, where the $K(E/n)$ profiles display a sustained increase (type A ions), an increase followed by a decrease (type B ions) or a sustained decrease (type C ions). Here we can observe

some of these behaviors. For example, the ions shown in Figure 3A and 3C follow a type C behavior with the reduced mobility becoming lower with an increase in the field over concentration. This is the typical behavior of medium to large ions at room gas temperature. The explanation of the reduction in reduced mobility has to do with the increase in momentum transfer due to the increase in relative kinetic energies at high fields. Other behaviors however are apparent for other cases(V. D. Gandhi & Larriba-Andaluz, 2021). Figure 3D showcases a series of smaller ions (higher reduced mobilities) that contain at least one visible hump and can be difficult to classify as they are a mix between type C and type B ions where the reduced mobility at some point increases and then decreases. A very clear example of type B ion is tetramethylammonium (TMA) in Figure 3B. The reason for the hump has been explained previously and is related to the ion-induced dipole potential(V. D. Gandhi & Larriba-Andaluz, 2021). The idea is that at low fields, the ion-induced dipole interaction is stronger compared to the relative kinetic energy and is able to capture gas molecules at moderate distances compared to the physical radius of the molecule. As the field increases, the relative kinetic energy increases, reducing the effective capture radius of the ion and increasing the mobility in the process. Eventually, at high fields, the effect of the interaction is negligible compared to the kinetic energy and the reduced mobility decreases due to higher momentum transfer owing to higher energetic collision (type C behavior).

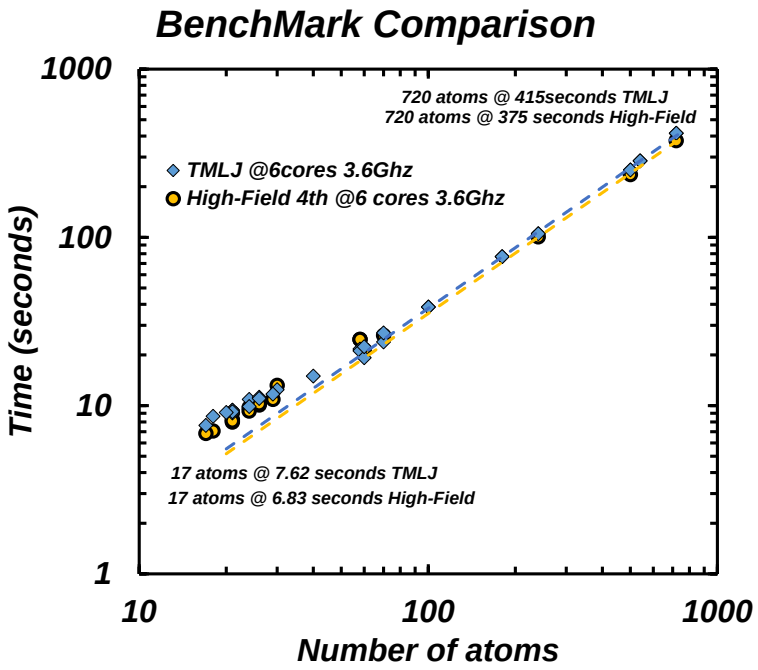

Figure 5. Benchmark Comparison for the High-Field 4-6-12 method as well as the regular TMLJ method for a 3.6Ghz cpu using 6 cores.

Given that the Trajectory Method has the ion-induced dipole potential (proportional to r^{-4}) as well as the induced dipole-induced dipole potential (dispersion force, proportional to r^{-6}), one should expect both effects to have a contribution to the enhanced capture radius. At 300K, however, it seems clear that the effect is mostly only visible for the ion-induced potential interaction as previously demonstrated in (V. D. Gandhi & Larriba-Andaluz, 2021). Figure 4 shows the reduced mobility as a function of the field over concentration for a gas temperature of 100K. While the largest ions seem to still behave as type C ions, as shown in Figure 4B, smaller ions Figure 4 A, B, and D have quite different behaviors. Many of the ions show two humps instead of one. Once again, the simplest ion to follow is TMA. The first drop in the reduced mobility (0 to 30Td) corresponds to an increase in momentum transfer due to an increase in field. As 30Td is reached, part of the effective capture radius due to r^{-6} potential is reduced leading to the first hump between 30 and 70Td. After 70Td, the second part of the effective capture radius due to r^{-4} potential begins to shrink leading to the increase in reduced mobility. The ion becomes the most mobile at 115Td after which

hard sphere momentum transfer dominates. This is the first time that a double hump (almost a triple hump if the first portion is considered) is shown in a high field calculation for polyatomic ions with such detail. We will label this type of interactions as type D to follow with previous nomenclature. This new behavior of the ion brings about different possibilities of separation that where not possible previously. For example, Naphthalene and Choline at 100K are barely separable at zero field. However, their behavior is very different as the field increases, having the largest separation at 80Td as shown in Figure 4D. Similarly, phenanthrene and anthracene are difficult to separate at low mobility, but the separation becomes larger at 40Td. Note that these curves have been obtained numerically assuming a 4-6-12 interaction only. It may be possible that higher-order interactions like ion quadrupole interaction, neutral dipole interactions or even quantum interactions may also be observable at such temperatures that could lead to somewhat different curves. Furthermore, the use of even heavier gases with larger polarizabilities (such as CO_2) may lead to even more clear separations between the different potential interactions. It is also expected that the inelasticity of the collisions, which is not yet considered here may have an impact at high fields.

Regarding the speed of the new high-field algorithms, Figure 5 shows the benchmark comparison for several ions. The algorithm performs in general around 10-20% percent faster than the regular 4-6-12 TMLJ algorithm for the same cases (zero field and room temperature). The improvement in speed has to do mostly with more efficient coding which will eventually be added to the regular TMLJ subroutine. After the deflection angle calculation is completed, adding results from higher-order approximations is nearly instantaneous for any ion.

The code can be downloaded free of charge[1].

5. Conclusions

A parallelized tool to calculate ion mobility at high fields using the two-temperature theory has been implemented in the program IMoS. The resulting theory has been tested against available experimental data for small ions in light gases yielding quite promising results. Calculations for heavier gases and different gas temperatures has also been implemented even though there is insufficient experimental data to fully assess the results. The results however are within what should be expected for room temperature gases, with the caveat that no inelasticity is considered for the time being. Testing the algorithm at lower temperatures produces some very interesting variations in the mobility, including double humps in some of the small ions. Closer inspection reveals that each of the humps pertains to the reduction of the capture radius, starting first with that of the dispersion forces and followed by the ion-induced dipole interaction. Other interactions not considered here may have their own effect so it is crucial that empirical results are provided before the calculations can be further optimized at these temperatures. However, the fact that different interactions can be observed for different fields at low temperature has many implications including separations of observable interactions and quantized effects. Once sufficient data is available, the study of the interactions may be improved substantially.

6. Conflict of interest

The authors declare no competing interest.

7. Acknowledgements

The authors would like to thank Iain Campuzano for providing the DFT calculations used to optimize some of the L-J potentials that IMoS uses(Campuzano et al., 2012). The author would finally like to acknowledge CDSE NSF grant ID: 1904879 and ID: 2203968.

8. Supporting Information

[1] www.imospedia.com/download-area.

An updated manual of IMoS v1.12 with examples of how to run the algorithm for high-field calculations.

9. References

Campuzano, I., Bush, M. F., Robinson, C. V., Beaumont, C., Richardson, K., Kim, H., & Kim, H. I. (2012). Structural characterization of drug-like compounds by ion mobility mass spectrometry: comparison of theoretical and experimentally derived nitrogen collision cross sections. *Analytical chemistry, 84*(2), 1026-1033.

Chapman, S., & Cowling, T. G. (1970). *The mathematical theory of non-uniform gases: an account of the kinetic theory of viscosity, thermal conduction and diffusion in gases*: Cambridge university press.

Coots, J., Gandhi, V., Onakoya, T., Chen, X., & Andaluz, C. L. (2020). A parallelized tool to calculate the electrical mobility of charged aerosol nanoparticles and ions in the gas phase. *Journal of Aerosol Science*, 105570.

Dodds, J. N., & Baker, E. S. (2019). Ion Mobility Spectrometry: Fundamental Concepts, Instrumentation, Applications, and the Road Ahead. *J Am Soc Mass Spectrom, 30*(11), 2185-2195. doi: 10.1007/s13361-019-02288-2

Donald, W. A., & Prell, J. (2019). *Advances in Ion Mobility-Mass Spectrometry: Fundamentals, Instrumentation and Applications*: Elsevier.

Epstein, P. S. (1924). On the resistance experienced by spheres in their motion through gases. *Physical Review, 23*(6), 710.

Gabelica, V., & Marklund, E. (2018). Fundamentals of ion mobility spectrometry. *Current opinion in chemical biology, 42*, 51-59.

Gandhi, V. (2022). A Critical Review of the two-temperature theory and the derivation of matrix elements. High field Ion mobility and energy calculation for all-atom structures in light gases using a 4-6-12 potential. [Review]. *submitted*.

Gandhi, V. D., & Larriba-Andaluz, C. (2021). Predicting ion mobility as a function of the electric field for small ions in light gases. *Analytica Chimica Acta*, 339019.

Garcia- Ybarra, P., & Rosner, D. E. (1989). Thermophoretic properties of nonspherical particles and large molecules. *AIChE Journal, 35*(1), 139-147.

Kim, H., Kim, H. I., Johnson, P. V., Beegle, L. W., Beauchamp, J., Goddard, W. A., & Kanik, I. (2008). Experimental and theoretical investigation into the correlation between mass and ion mobility for choline and other ammonium cations in N2. *Analytical chemistry, 80*(6), 1928-1936.

Kruger, C. H., & Vincenti, W. (1965). Introduction to physical gas dynamics. *John Wlley & Sons*.

Larriba-Andaluz, C. (2021). A perspective on the theoretical and numerical aspects of Ion Mobility Spectrometry. *International Journal of Mass Spectrometry*, 116719.

Larriba-Andaluz, C., Fernandez-Garcia, J., Ewing, M. A., Hogan, C. J., & Clemmer, D. E. (2015). Gas molecule scattering & ion mobility measurements for organic macro-ions in He versus N 2 environments. *Physical Chemistry Chemical Physics, 17*(22), 15019-15029.

Larriba, C., & Hogan Jr, C. J. (2013a). Free molecular collision cross section calculation methods for nanoparticles and complex ions with energy accommodation. *Journal of Computational Physics, 251*, 344-363.

Larriba, C., & Hogan Jr, C. J. (2013b). Ion mobilities in diatomic gases: measurement versus prediction with non-specular scattering models. *The Journal of Physical Chemistry A, 117*(19), 3887-3901.

Mackowski, D. W. (2006). Monte Carlo simulation of hydrodynamic drag and thermophoresis of fractal aggregates of spheres in the free-molecule flow regime. *Journal of Aerosol Science, 37*(3), 242-259.

Mason, E. A., & Schamp Jr, H. W. (1958). Mobility of gaseous Ions in weak electric fields. *Annals of physics, 4*(3), 233-270.

McDaniel, E. W., & Mason, E. A. (1973). Mobility and diffusion of ions in gases.

Mesleh, M. F., Hunter, J. M., Shvartsburg, A. A., Schatz, G. C., & Jarrold, M. F. (1996). Structural information from ion mobility measurements: Effects of the long-range potential. *Journal of Physical Chemistry, 100*(40), 16082-16086.

Rus, J., Moro, D., Sillero, J. A., Royuela, J., Casado, A., Estevez-Molinero, F., & de la Mora, J. F. (2010). IMS–MS studies based on coupling a differential mobility analyzer (DMA) to commercial API–MS systems. *International Journal of Mass Spectrometry, 298*(1-3), 30-40.

Shrivastav, V., Nahin, M., Hogan, C. J., & Larriba-Andaluz, C. (2017). Benchmark comparison for a multi-processing ion mobility calculator in the free molecular regime. *Journal of the American Society for Mass Spectrometry, 28*(8), 1540-1551.

Viehland, L. A., & Mason, E. (1975). Gaseous lon mobility in electric fields of arbitrary strength. *Annals of Physics, 91*(2), 499-533.

Viehland, L. A., & Mason, E. (1978). Gaseous ion mobility and diffusion in electric fields of arbitrary strength. *Annals of Physics, 110*(2), 287-328.

Viehland, L. A., & Viehland, L. A. (2018). *Gaseous ion mobility, diffusion, and reaction*: Springer.

Wannier, G. H. (1953). Motion of gaseous ions in strong electric fields. *The Bell System Technical Journal, 32*(1), 170-254.

Figures

Figure 1

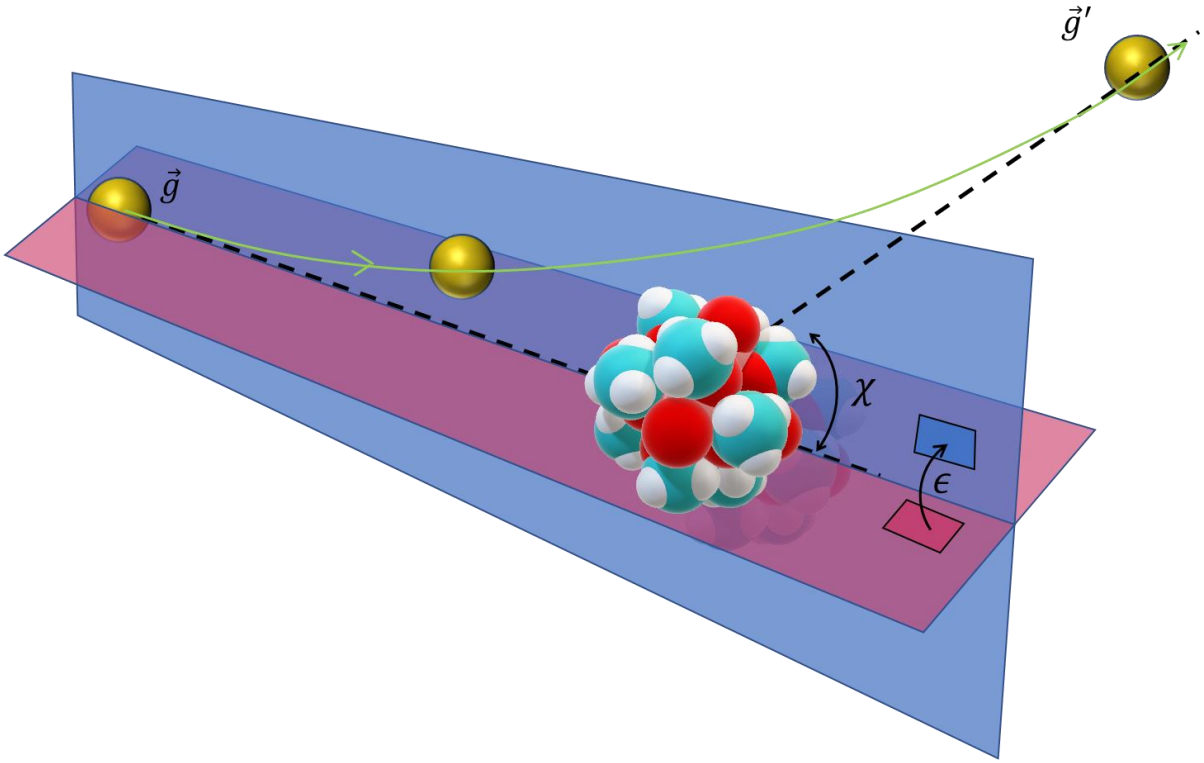

Figure 1. Representation of a gas-ion trajectory in 3D. The gas molecule with the velocity $\vec{g}$ is being deflected by an angle χ. The trajectory plane (blue) makes an angle ϵ with respect to a fixed reference plane (red). (Adapted from Vincenti and Kruger[74], and Larriba and Prell[9]).

Figure 2

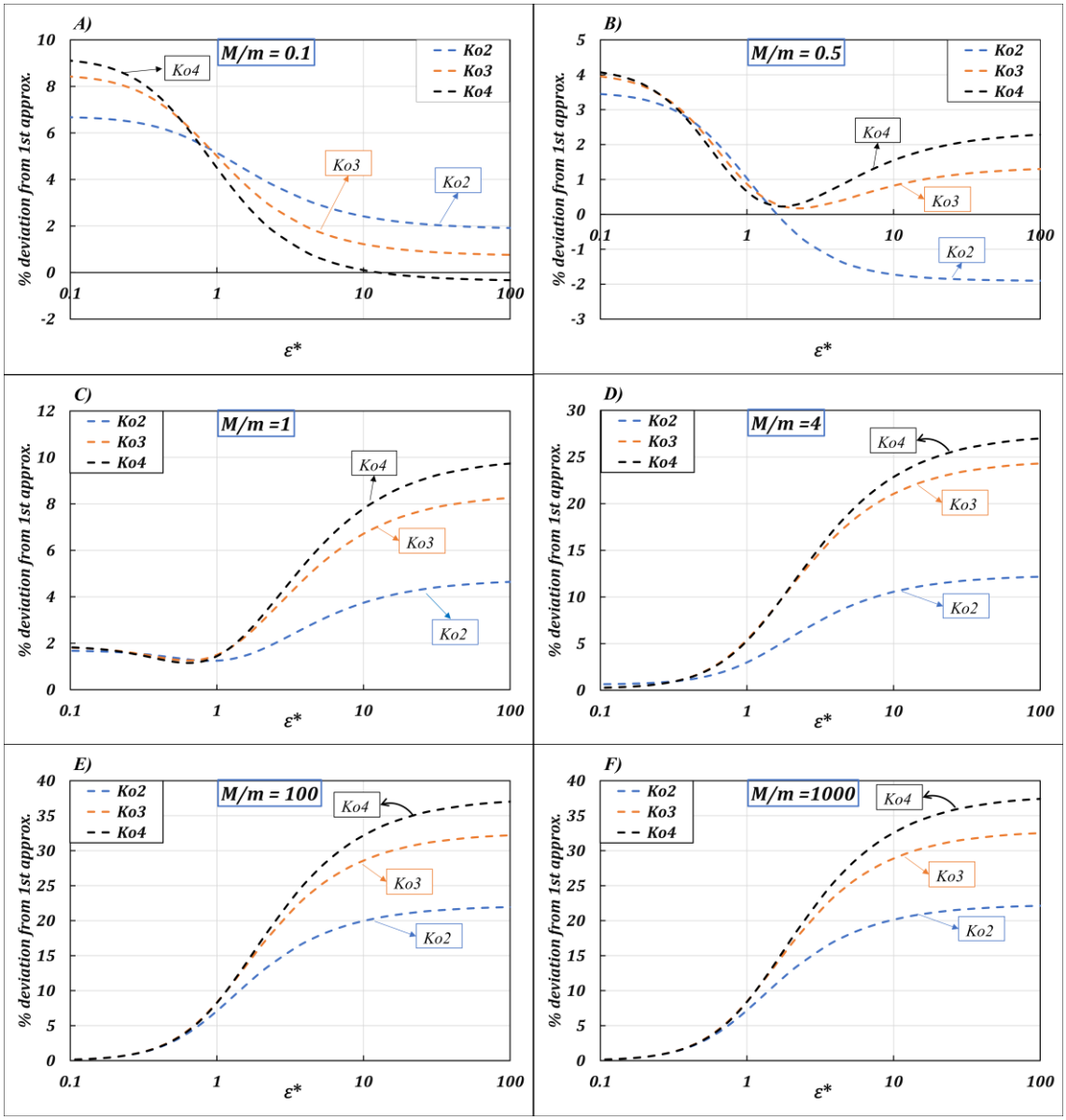

Figure 2. The percentage difference between the first and the higher order approximations (for the hard sphere model) as a function of the dimensionless parameter $\mathcal{E}^*$ at different mass ratios (A) $M/m = 0.1$, (B) $M/m = 0.5$, (C) $M/m = 1$, (D) $M/m = 4$, (E) $M/m = 100$, (F) $M/m = 1000$. The y-axis is given by $\%\, deviation = \frac{(\langle v_d \rangle_x - \langle v_d \rangle_I) \times 100}{\langle v_d \rangle_I}$. Calculations were performed in IMoS [86-89].

Figure 3 and 4

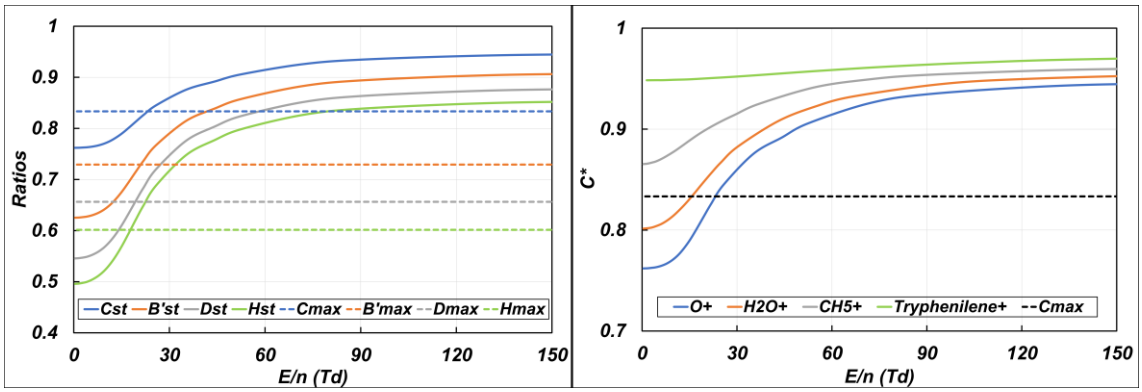

Figure 3. CCS ratios for O^+ ion in helium gas as a function of E/n. The dashed and solid lines represent the CCS ratios for the Maxwell and 4-6-12 potential approximation model respectively.

Figure 4. C ratios for different ions in helium gas as a function of E/n. The dashed line represents the C* ratio for the Maxwell model. The C* ratio becomes closer to 1 at low E/n as the ion size increases.*

Figure 5

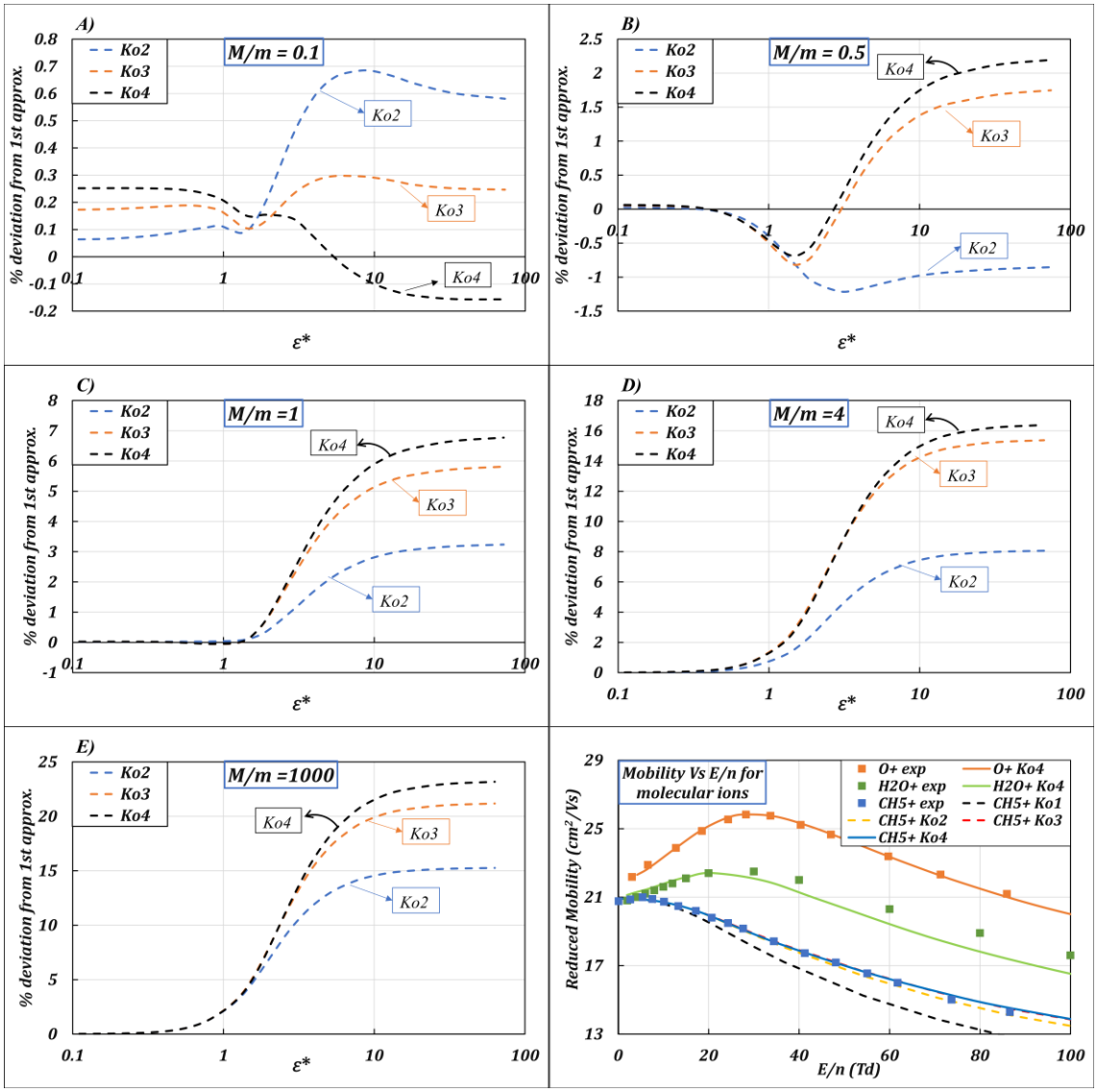

Figure 5. The percentage difference between the first and the higher order approximations (using the 4-6-12 Lennard-Jones trajectory method) as a function of the dimensionless parameter $\mathcal{E}^*$ at different mass ratios (A) $M/m = 0.1$, (B) $M/m = 0.5$, (C) $M/m = 1$, (D) $M/m = 4$, (E) $M/m = 1000$. The y-axis is given by $\%\ deviation = \frac{(\langle v_d \rangle_x - \langle v_d \rangle_I) \times 100}{\langle v_d \rangle_I}$. Figure 5F shows the experimental and the calculated mobility for O^+, H_2O^+ and CH_5^+ in helium as a function of E/n. For CH_5^+, the mobility using different approximations is illustrated. Calculations were performed in IMoS [86-89].

Figure captions

Figure 1. Representation of a gas-ion trajectory in 3D. The gas molecule with the velocity $\vec{g}$ is being deflected by an angle χ. The trajectory plane (blue) makes an angle ϵ with respect to a fixed reference plane (red). (Adapted from Vincenti and Kruger[74], and Larriba and Prell[9]).

Figure 2. The percentage difference between the first and the higher order approximations (for the hard sphere model) as a function of the dimensionless parameter $\mathcal{E}^*$ at different mass ratios (A) $M/m = 0.1$, (B) $M/m = 0.5$, (C) $M/m = 1$, (D) $M/m = 4$, (E) $M/m = 100$, (F) $M/m = 1000$. The y-axis is given by $\%\, deviation = \frac{(\langle v_d \rangle_x - \langle v_d \rangle_I) \times 100}{\langle v_d \rangle_I}$. Calculations were performed in IMoS[86-89].

Figure 3. CCS ratios for O^+ ion in helium gas as a function of E/n. The dashed and solid lines represent the CCS ratios for the Maxwell and 4-6-12 potential approximation model respectively.

Figure 4. *C** ratios for different ions in helium gas as a function of E/n. The dashed line represents the *C** ratio for the Maxwell model. The *C** ratio becomes closer to 1 at low E/n as the ion size increases.

Figure 5. The percentage difference between the first and the higher order approximations (using the 4-6-12 Lennard-Jones trajectory method) as a function of the dimensionless parameter $\mathcal{E}^*$ at different mass ratios (A) $M/m = 0.1$, (B) $M/m = 0.5$, (C) $M/m = 1$, (D) $M/m = 4$, (E) $M/m = 1000$. The y-axis is given by $\%\, deviation = \frac{(\langle v_d \rangle_x - \langle v_d \rangle_I) \times 100}{\langle v_d \rangle_I}$. Figure 5F shows the experimental and the calculated mobility for O^+, H_2O^+ and CH_5^+ in helium as a function of E/n. For CH_5^+, the mobility using different approximations is illustrated. Calculations were performed in IMoS[86-89].